Multidimensional Low-Rank Representation for Sparse Hyperspectral Unmixing

Ling Wu, Jie Huang, Ming-Shuang Guo

***Abstract*—Hyperspectral unmixing is aimed at identifying pure materials in hyperspectral images as well as their relative proportions within each pixel. In light of the high similarity of spectral signatures among neighboring pixels, a low-rank property is proposed as a prior to enhance the abundance estimation results. In the previous studies, however, the low-rank prior is only reflected in the low-rank constraint on the abundance matrix. In this letter, we present a multidimensional low-rank model for the hyperspectral unmixing problem. We first reshape the abundance matrix to a 3-D abundance tensor. Then we simultaneously impose low-rank constraints on different modes of the abundance tensor to maximize the use of latent spatial information. Moreover, we incorporate the bilateral joint-sparse structure and derive a new algorithm, named as *multidimensional low-rank representation based sparse unmixing*. Experiments on both synthetic and real data demonstrate the effectiveness of the proposed algorithm.**

***Index Terms*—Hyperspectral unmixing, abundance tensor, multidimensional low-rank, bilateral joint-sparse.**

I. Introduction

HYPERSPECTRAL images (HSIs) are more detailed in terms of spectral and spatial information than standard images, which encourages their widespread use in different kinds of industries [1, 2]. However, the complexity and diversity of ground objects environment also limit the applications of the resulting HSIs. To address the problem, hyperspectral unmixing is introduced for extracting the pure materials (endmembers) mixed in an HSI, along with their proportions in each pixel (abundances) [3]. The linear mixing model (LMM) is widely used owing to its flexibility and decent performance. Additionally, the fractional abundances are assumed to follow the abundance nonnegative constraint (ANC) and the abundance sum-to-one constraint (ASC) by nature [4]. Extraction of endmembers plays a major role in the effectiveness of conventional research. Given the complex ground objects environment, a spectral library containing a plethora of reference spectra is suggested as an alternative.

To enhance the unmixing capacity, some priors are incorporated by scholars over the past years. For a single pixel, the size of the spectral library is much larger than the amount of pure materials involved in the composition, thus the inherent sparsity is introduced. To blend the sparse structure, Iordache *et al.* take the ℓ_1 norm as a convex replacement for the ℓ_0 regularization to avoid the NP-hard problem in [5]. And the alternating direction sparse and low-rank unmixing algorithm (ADSpLRU) proposes to use a weighted ℓ_1 norm as an alternant [6]. Nevertheless, considering only pixelwise regularization is hard to provide stable results, thus a joint $\ell_{2,1}$ norm is proposed for applying to all pixels [7]. What's more, the joint-sparse-blocks and low-rank unmixing algorithm (JSpBLRU) incorporates the local sparsity in blocks vertically [8], while the ensuing bilateral joint-sparse and low-rank unmixing algorithm (BiJSpLRU) [9] pays considerate attention to both the horizontal and vertical directions. As it turns out, they all yield positive results.

As adjacent pixels possess spectral similarity, the low-rank prior is obtained for the deep excavation of spectral and spatial information. The sparse unmixing via variable splitting augmented Lagrangian and total variation algorithm (SUnSAL-TV) implements the sparse prior with the addition of a total variation (TV) regularizer to activate the piecewise smooth in abundance maps [10]. To maximize the prior's mining, JSpBLRU and BiJSpLRU both build models by a weighted nuclear norm combined with some sort of sparse structures. Also, the weighted nuclear norm is employed in the weighted nonlocal low-rank tensor regularization in [11], which imposes low rankness on the mode-3 unfolding of the abundance matrix of the patch group tensor. Such a strategy achieves great promotion in the unmixing process. However, the above exploitation of low-rankness relies solely on the abundance matrix corresponding to the unfolding of the 3-D observed HSI along one mode.

In this article, we propose a multidimensional low-rank model for the hyperspectral unmixing problem. We first reshape the abundance matrix into a 3-D abundance tensor and then consider the low-rank property of matrices expanded by different modes of the abundance tensor. We solve the proposed model by a multidimensional low-rank representation (MdLRR) based sparse hyperspectral unmixing algorithm. It is worth mentioning that experimental results listed later demonstrate the superiority of our algorithm for hyperspectral unmixing.

The remainder of this paper is formed as follows. We describe the pertinent techniques used in our work in Section 2. In Section 3, we propose the multidimensional low-rank algorithm. Section 4 presents the experimental results on both synthetic and real data. Finally, we draw a conclusion in Section 5.

This research is supported in part by NSFC (Grant No. 12171072), in part by Key Projects of Applied Basic Research in Sichuan Province (Grant No. 2020YJ0216), in part by National Key Research and Development Program of China (Grant No. 2020YFA0714001), in part by the Fundamental Research Funds for the Central Universities (Grant No. ZYGX2019J093). *(Corresponding author: J. Huang.)*

The authors are with School of Mathematical Sciences/Research Center for Image and Vision Computing, University of Electronic Science and Technology of China, Chengdu, Sichuan, 611731, PR China (e-mail: huangjie_uestc@uestc.edu.cn)

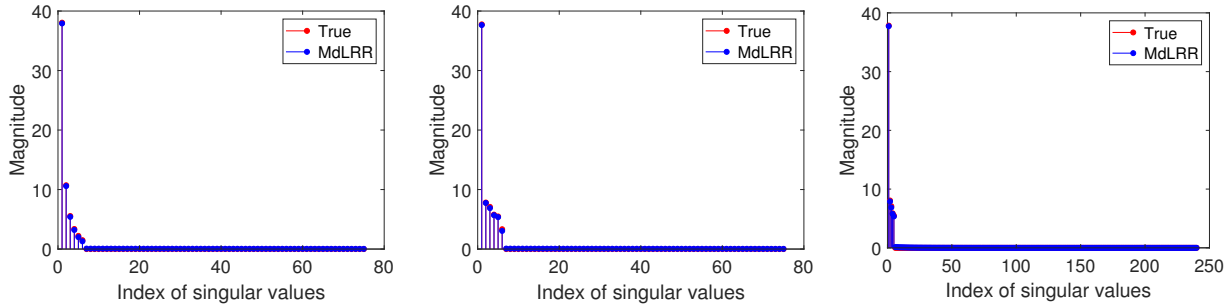

(a) mode-1 (b) mode-2 (c) mode-3

Fig. 1: Singular values of mode-n unfoldings of the abundance tensor for Synthetic data 1 with SNR $= 30$ dB.

II. Related Work

Let $\boldsymbol{\mathcal{Y}} \in \mathbb{R}^{s\times t\times L}$ represent the observed HSI with $s \times t$ pixels and L spectral bands and $\boldsymbol{Y} \in \mathbb{R}^{L\times N}$ be the mode-3 unfolding of $\boldsymbol{\mathcal{Y}}$ with $N = s \times t$. To maintain consistency with traditional terminology, we use tensor notations as described in [12]. The LMM considers

$$\boldsymbol{Y} = \boldsymbol{A}\boldsymbol{X} + \boldsymbol{E}, \tag{1}$$

or equivalently,

$$\boldsymbol{\mathcal{Y}} = \boldsymbol{\mathcal{X}} \times_3 \boldsymbol{A} + \boldsymbol{\mathcal{E}}, \tag{2}$$

where $\boldsymbol{A} \in \mathbb{R}^{L\times M}$ denotes the spectral dictionary with M endmembers, $\boldsymbol{X} \in \mathbb{R}^{M\times N}$ is the abundance matrix consisting of abundance vectors for those pixels, $\boldsymbol{\mathcal{X}} \in \mathbb{R}^{s\times t\times M}$ is the 3-D abundance tensor, and both $\boldsymbol{\mathcal{E}}$ and $\boldsymbol{E}$ stand for the noise. In order to take advantage of physical information, ANC and ASC are added and displayed as

$$\boldsymbol{X} \geq \boldsymbol{0}, \quad \boldsymbol{1}^T\boldsymbol{X} = \boldsymbol{1}^T, \tag{3}$$

respectively. In fact, we relax the ASC, according to interpretations in the literature [5–7].

After partitioning the abundance matrix as $\boldsymbol{X} = [\boldsymbol{X}_1, \ldots, \boldsymbol{X}_S]$, the JSpBLRU model is

$$\min_{\boldsymbol{X}\in\mathbb{R}_+^{M\times N}} \frac{1}{2}\|\boldsymbol{Y} - \boldsymbol{A}\boldsymbol{X}\|_F^2 + \lambda\sum_{j=1}^{S}\|\boldsymbol{X}_j\|_{\boldsymbol{W}_j,2,1} + \tau\|\boldsymbol{X}\|_{\boldsymbol{b},*} \tag{4}$$

where λ and τ are nonnegative regularization parameters, $\|\boldsymbol{X}_j\|_{\boldsymbol{W}_j,2,1} = \sum_{i=1}^{M} w_{ij}\|\boldsymbol{X}_j^{[i]}\|_2$, $\boldsymbol{X}_j^{[i]}$ is the ith row of the jth block of $\boldsymbol{X}$, $\boldsymbol{W} = [\boldsymbol{W}_1, \ldots, \boldsymbol{W}_S] = [w_{ij}] \in \mathbb{R}^{M\times S}$ is a nonnegative weighting matrix, S denotes the number of blocks, $\|\boldsymbol{X}\|_{\boldsymbol{b},*} = \sum_i b_i\sigma_i(\boldsymbol{X})$, $\sigma_i(\boldsymbol{X})$ is the ith singular value of $\boldsymbol{X}$, and $\boldsymbol{b} = [b_1, \ldots, b_r]$ is a nonnegative weighting vector with r being the rank of $\boldsymbol{X}$.

The bilateral joint-sparse structure is developed based on the joint-sparse structure, which further utilizes the sparse prior [9]. After partitioning the abundance matrices which have been unfolded along both the vertical and horizontal directions, the BiJSpLRU suggests utilizing the joint-sparse-block structure in the two directions. Define

$$\mathcal{J}_{S,\boldsymbol{W}}(\boldsymbol{X}) = \sum_{j=1}^{S}\|(\boldsymbol{X}\boldsymbol{P})_j\|_{(\boldsymbol{W}_1)_j,2,1} + \sum_{j=1}^{S}\|\boldsymbol{X}_j\|_{(\boldsymbol{W}_2)_j,2,1} \tag{5}$$

where $\boldsymbol{P}$ serves as a permutation matrix, then we can rewrite the BiJSpLRU unmixing model as

$$\min_{\boldsymbol{X}\in\mathbb{R}_+^{M\times N}} \frac{1}{2}\|\boldsymbol{Y} - \boldsymbol{A}\boldsymbol{X}\|_F^2 + \lambda\mathcal{J}_{S,\boldsymbol{W}}(\boldsymbol{X}) + \tau\|\boldsymbol{X}\|_{\boldsymbol{b},*}. \tag{6}$$

Clearly, both JSpBLRU and BiJSpLRU only consider the low-rank property of $\boldsymbol{X}$, the mode-3 unfolding of $\boldsymbol{\mathcal{X}}$. In the following, we will present a multidimensional low-rank unmixing algorithm.

III. Proposed Algorithm

It is known that the abundance matrix $\boldsymbol{X}$, corresponding to the mode-3 unfolding $\boldsymbol{Y}$ of $\boldsymbol{\mathcal{Y}}$, has a clear low-rank property. In fact, we observe that the mode-1 and mode-2 unfoldings also admit the low-rank properties. For illustration, Fig. 1 shows that the three unfoldings of the abundance tensor by different modes all exist a low-rankness property. In this vein, we propose to impose a multidimensional low-rank regularization on the abundance tensor for spectral unmixing, so we can exploit the low-rank property of the abundance tensor at a deeper level. More specifically, we propose simultaneously regularizing the expansion matrices of the abundance tensor over the three modes, and denote the regularization term as

$$\mathcal{L}_{\boldsymbol{b}}(\boldsymbol{\mathcal{X}}) = \sum_{l=1}^{3}\|\boldsymbol{X}_{(l)}\|_{\boldsymbol{b}_l,*} \tag{7}$$

where $\boldsymbol{X}_{(l)}$ denotes the mode-l unfolding of $\boldsymbol{\mathcal{X}}$ and $\boldsymbol{b}_l$ are nonnegative weighting vectors, for $l = 1, 2, 3$. Combining the multidimensional low-rank property and the bilateral joint-sparse structure, we propose an unmixing model as

$$\min_{\boldsymbol{X}\in\mathbb{R}_+^{M\times N}} \frac{1}{2}\|\boldsymbol{Y} - \boldsymbol{A}\boldsymbol{X}\|_F^2 + \lambda\mathcal{J}_{S,\boldsymbol{W}}(\boldsymbol{X}) + \tau\mathcal{L}_{\boldsymbol{b}}(\boldsymbol{\mathcal{X}}). \tag{8}$$

Now we solve the model under the alternating direction multiplier method (ADMM) framework [13]. First, let us introduce auxiliary variables $\boldsymbol{\mathcal{V}}_l$ and their mode-j unfoldings $\boldsymbol{V}_{l,(j)}$ for $l = 1, \ldots, 6$, $j = 1, 2$. For simplicity, we denote the mode-3 unfolding of $\boldsymbol{\mathcal{V}}_i$ as $\boldsymbol{V}_i$. After partitioning $\boldsymbol{V}_1$ and $\boldsymbol{V}_2$ as $\boldsymbol{V}_l = [\boldsymbol{V}_{l,1}, \ldots, \boldsymbol{V}_{l,S}]$ for $l = 1, 2$, which is similarly to $\boldsymbol{X}\boldsymbol{P}$ and $\boldsymbol{X}$, we equivalently have

$$\begin{aligned}\min_{\boldsymbol{X},\boldsymbol{V}_1,\ldots,\boldsymbol{V}_6}\ & \frac{1}{2}\|\boldsymbol{Y} - \boldsymbol{A}\boldsymbol{X}\|_F^2 + \lambda\sum_{l=1}^{2}\sum_{j=1}^{S}\|\boldsymbol{V}_{l,j}\|_{(\boldsymbol{W}_l)_j,2,1} \\ & + \tau\sum_{l=1}^{3}\|\boldsymbol{V}_{l+2,(l)}\|_{\boldsymbol{b}_l,*} + \iota_{\mathbb{R}^+}(\boldsymbol{V}_6) \\ \text{s.t.}\ & \boldsymbol{X}\boldsymbol{P} = \boldsymbol{V}_1,\ \boldsymbol{X} = \boldsymbol{V}_l,\ l = 2, \ldots, 6\end{aligned} \tag{9}$$

where ι_Ω is the indicator function of the set Ω, i.e., if $x \in \Omega$, $\iota_\Omega(x) = 0$, $\iota_\Omega(x) = +\infty$ otherwise. For a more concise

expression, we specify

$$g(\boldsymbol{X},\boldsymbol{V}) = \frac{1}{2}\|\boldsymbol{Y}-\boldsymbol{A}\boldsymbol{X}\|_F^2 + \lambda\sum_{l=1}^{2}\sum_{j=1}^{S}\|\boldsymbol{V}_{l,j}\|_{(\boldsymbol{W}_l)_j,2,1} + \tau\sum_{l=1}^{3}\|\boldsymbol{V}_{l+2,(l)}\|_{\boldsymbol{b}_l,*} + \iota_{\mathbb{R}^+}(\boldsymbol{\mathcal{V}_6}) \tag{10}$$

and set $\boldsymbol{V}=[\boldsymbol{V}_1\ \boldsymbol{V}_2\ \boldsymbol{V}_3\ \boldsymbol{V}_4\ \boldsymbol{V}_5\ \boldsymbol{V}_6]$, $\boldsymbol{G}=[\boldsymbol{P}\ \boldsymbol{I}\ \boldsymbol{I}\ \boldsymbol{I}\ \boldsymbol{I}\ \boldsymbol{I}]$, hence we simplify the optimization problem as a compact form

$$\begin{aligned}\min_{\boldsymbol{X},\boldsymbol{V}}\quad & g(\boldsymbol{X},\boldsymbol{V})\\ s.t.\quad & \boldsymbol{X}\boldsymbol{G}=\boldsymbol{V}.\end{aligned} \tag{11}$$

By assigning

$$\mathcal{L}_\mu(\boldsymbol{X},\boldsymbol{V};\boldsymbol{\Lambda}) = g(\boldsymbol{X},\boldsymbol{V}) + \frac{\mu}{2}\|\boldsymbol{X}\boldsymbol{G}-\boldsymbol{V}-\boldsymbol{\Lambda}\|_F^2 \tag{12}$$

where $\mu>0$ is a penalty parameter and $\boldsymbol{\Lambda}=[\boldsymbol{\Lambda}_1,\ldots,\boldsymbol{\Lambda}_6]$, we derive the ADMM framework

$$\begin{cases}\boldsymbol{X}^{k+1} &= \arg\min_{\boldsymbol{X}} \mathcal{L}_\mu(\boldsymbol{X},\boldsymbol{V}^k;\boldsymbol{\Lambda}^k)\\ \boldsymbol{V}^{k+1} &= \arg\min_{\boldsymbol{V}} \mathcal{L}_\mu(\boldsymbol{X}^{k+1},\boldsymbol{V};\boldsymbol{\Lambda}^k)\\ \boldsymbol{\Lambda}^{k+1} &= \boldsymbol{\Lambda}^k-(\boldsymbol{X}^{k+1}\boldsymbol{G}-\boldsymbol{V}^{k+1}).\end{cases} \tag{13}$$

To make this letter self-contained, we define the vect-soft operator and the singular value thresholding operator by

$$\begin{aligned}&\textbf{vect-soft}_\alpha(\boldsymbol{x}) = \boldsymbol{x}\frac{\max\{\|\boldsymbol{x}\|_2-\alpha,0\}}{\max\{\|\boldsymbol{x}\|_2-\alpha,0\}-\alpha},\\ &\textbf{SVT}_{\boldsymbol{b},\beta}(\boldsymbol{X}) = \boldsymbol{U}\boldsymbol{Diag}((\sigma_1-\beta b_1)_+,\ldots,(\sigma_r-\beta b_r)_+)\boldsymbol{V}^T,\end{aligned} \tag{14}$$

where $(\cdot)_+=\textbf{max}(\cdot,0)$ and $\boldsymbol{X}=\boldsymbol{U}\boldsymbol{Diag}(\sigma_1,\ldots,\sigma_r)\boldsymbol{V}^T$ is the SVD of $\boldsymbol{X}$. Let $\varepsilon=10^{-16}$ be a small constant used for avoiding singularities. Finally, we summarize the proposed MdLRR in Algorithm 1.

Algorithm 1: Pseudocode of the MdLRR Algorithm

Input: $\boldsymbol{Y}$, $\boldsymbol{A}$.
Selected parameters: λ, τ, and μ.
Initialization: $\boldsymbol{V}_l^0$, $\boldsymbol{\Lambda}_l^0$, $l=1,\ldots,6$, and set $k=0$.
Repeat:
Compute $\boldsymbol{X}^{k+1}$ by
$\boldsymbol{X}^{k+1}=(\boldsymbol{A}^T\boldsymbol{A}+6\mu\boldsymbol{I})^{-1}(\boldsymbol{A}^T\boldsymbol{Y}+\mu((\boldsymbol{V}_1^k+\boldsymbol{\Lambda}_1^k)\boldsymbol{P}^T+\sum_{l=2}^{6}(\boldsymbol{V}_l^k+\boldsymbol{\Lambda}_l^k)))$.
Compute $\boldsymbol{W}_{\tilde{l}}^{k+1}$ and $\boldsymbol{b}_l^{k+1}$ by
$(\boldsymbol{W}_1^{k+1})_{ij}=\frac{1}{\|((\boldsymbol{X}^{k+1}\boldsymbol{P})_j-\boldsymbol{\Lambda}_{1,j}^k)^{[i]}\|_2+\varepsilon}$
$(\boldsymbol{W}_2^{k+1})_{ij}=\frac{1}{\|(\boldsymbol{X}_j^{k+1}-\boldsymbol{\Lambda}_{2,j}^k)^{[i]}\|_2+\varepsilon}$
$(\boldsymbol{b}_l^{k+1})_j=\frac{1}{\sigma_j(\boldsymbol{X}_{(l)}^{k+1}-\boldsymbol{\Lambda}_{l+2,(l)}^k)+\varepsilon}$ for $l=1,2,3$.
Compute $\boldsymbol{V}_l^{k+1}$ by
$(\boldsymbol{V}_{1,j}^{k+1})^{[i]}=\textbf{vect-soft}_{\frac{\lambda}{\mu}(\boldsymbol{W}_1^{k+1})_{ij}}(((\boldsymbol{X}^{k+1}\boldsymbol{P})_j-\boldsymbol{\Lambda}_{1,j}^k)^{[i]})$
$(\boldsymbol{V}_{2,j}^{k+1})^{[i]}=\textbf{vect-soft}_{\frac{\lambda}{\mu}(\boldsymbol{W}_2^{k+1})_{ij}}((\boldsymbol{X}_j^{k+1}-\boldsymbol{\Lambda}_{2,j}^k)^{[i]})$
$\boldsymbol{V}_{l+2,(l)}^{k+1}=\textbf{SVT}_{\boldsymbol{b}_l^{k+1},\frac{\tau}{\mu}}(\boldsymbol{X}_{(l)}^{k+1}-\boldsymbol{\Lambda}_{l+2,(l)}^k)$, $l=1,2,3$
$\boldsymbol{V}_6^{k+1}=\textbf{max}(\boldsymbol{X}^{k+1}-\boldsymbol{\Lambda}_6^k,\boldsymbol{0})$.
Compute $\boldsymbol{\Lambda}_l^{k+1}$ by
$\boldsymbol{\Lambda}_1^{k+1}=\boldsymbol{\Lambda}_1^k-(\boldsymbol{X}^{(k+1)}\boldsymbol{P}-\boldsymbol{V}_1^{k+1})$
$\boldsymbol{\Lambda}_l^{k+1}=\boldsymbol{\Lambda}_l^k-(\boldsymbol{X}^{(k+1)}-\boldsymbol{V}_l^{k+1})$, $l=2,\ldots,6$.
Until some stopping criterion is satisfied.
Output: $\hat{\boldsymbol{X}}=\boldsymbol{X}^{k+1}$.

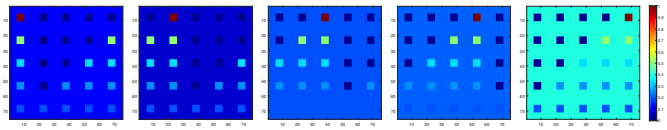

Fig. 2: True abundance maps for endmembers #1-#5 for Synthetic data 1.

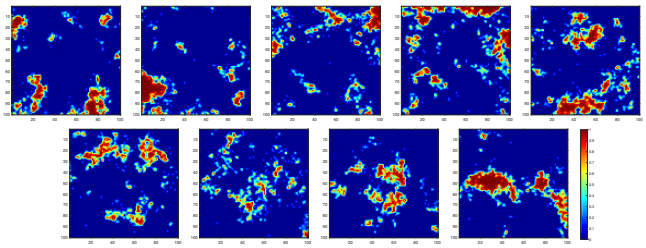

Fig. 3: True abundance maps for (top row) endmembers #1-#5 and (bottom row) endmembers #6-#9 for Synthetic data 2.

IV. Experiments

This section illustrates the efficiency of the proposed algorithm on both synthetic and real data. We use the signal-to-reconstruction error (SRE) and the root mean square error (RMSE) as metrics to evaluate the experimental performance, which are defined by

$$\text{SRE(dB)} = 10\log_{10}\frac{\|\boldsymbol{X}\|_F^2}{\|\hat{\boldsymbol{X}}-\boldsymbol{X}\|_F^2},\ \text{RMSE} = \frac{1}{\sqrt{MN}}\|\hat{\boldsymbol{X}}-\boldsymbol{X}\|_F, \tag{15}$$

where we describe the real and estimated abundance matrices with respect to N pixels via $\boldsymbol{X}$ and $\hat{\boldsymbol{X}}$ separately, M is the number of endmembers. Generally, one algorithm offers better results when the SRE is higher and the RMSE is lower. Comparisons are conducted with several classic algorithms, including SUnSAL-TV, ADSpLRU, JSpBLRU, BiJSpLRU. The series of parameters are referred to as in [9] and best results are recorded for each algorithm. Our tests are completed by using MATLAB R2019a on a desktop with 3.60 GHz Intel Core i9-9900K and 32 GB memory.

A. *Simulated experiments*

We conduct experiments on two sets of simulated data:

- **Synthetic data 1:** The first data cube includes 75×75 pixels with 240 bands per pixel. The spectral library $\boldsymbol{A}\in\mathbb{R}^{224\times240}$ is a portion of the U.S. Geological Survey (USGS) spectral library. According to LMM, we generate the dataset by randomly selecting five endmembers from $\boldsymbol{A}$ and the true abundance maps are shown in Fig. 2. Furthermore, the true data cube is distributed by white Gaussian i.i.d. noise with SNR $=$ 20, 30, and 40 dB, respectively.
- **Synthetic data 2:** The second data cube has 100×100 pixels with 99 bands per pixel. The spectral library comes from the National Aeronautics and Space Administration Johnson Space Center Spacecraft materials Spectral Database. For the creation of the true data cube, we randomly pick nine endmembers with their true abundance

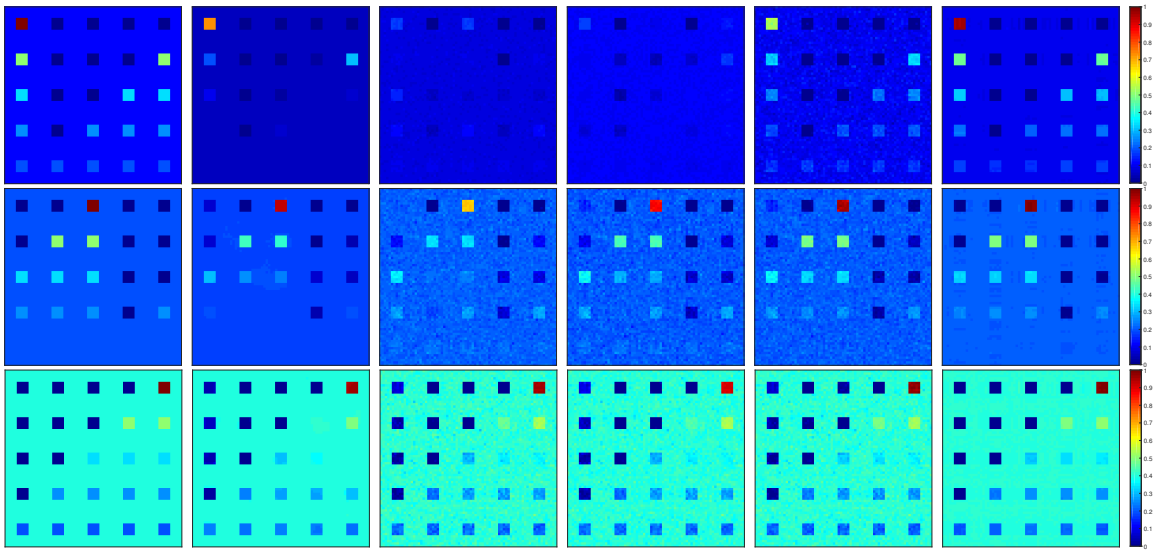

Fig. 4: True and estimated abundance maps by different unmixing algorithms for Synthetic data 1 with SNR = 30 dB.

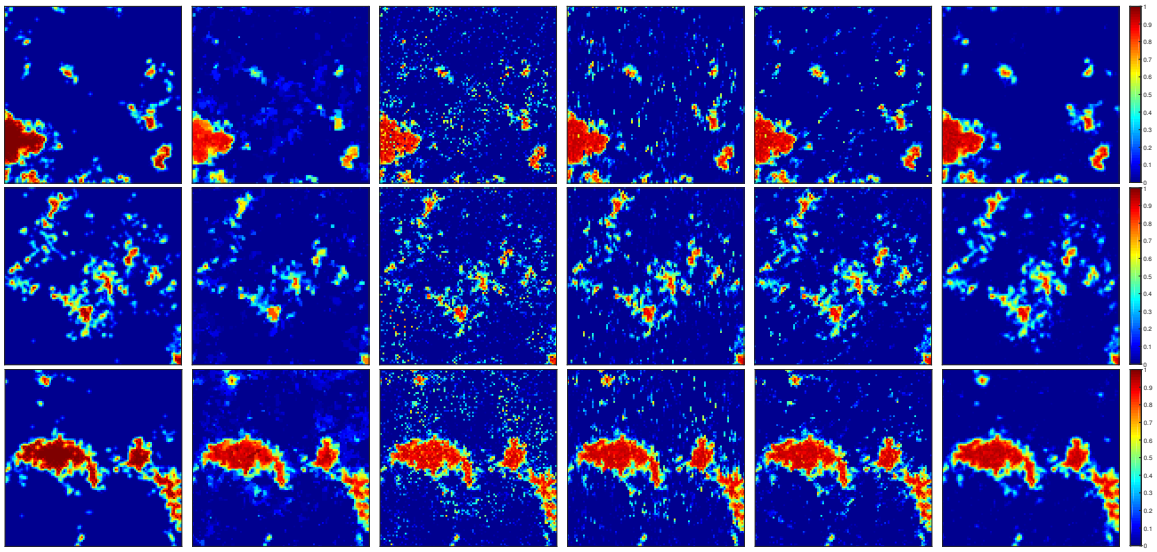

Fig. 5: True and estimated abundance maps by different unmixing algorithms for Synthetic data 2 with SNR = 20 dB.

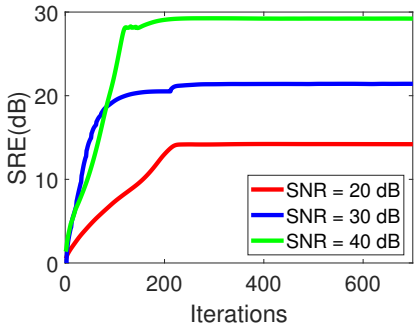

Fig. 6: Plot of SRE (dB) against iteration by MdLRR for Synthetic data 2.

maps shown in Fig. 3. After that, the true data cube is contaminated by white Gaussian i.i.d. noise with the same SNR values adopted for Synthetic data 1.

Figs. 4 and 5 show the abundance maps by different

TABLE I: SRE(dB) and RMSE values by different algorithms at different noise levels for Synthetic data 1 and 2.

Synthetic data 1						
Algorithm	SNR = 20 dB		SNR = 30 dB		SNR = 40 dB	
	SRE	RMSE	SRE	RMSE	SRE	RMSE
SUnSAL-TV	8.80	0.0125	14.94	0.0062	23.66	0.0023
ADSpLRU	8.09	0.0136	14.57	0.0065	32.59	0.0008
JSpBLRU	9.25	0.0119	15.64	0.0057	33.16	0.0008
BiJSpLRU	9.14	0.0121	19.39	0.0037	33.33	0.0007
MdLRR	**10.90**	**0.0098**	**27.62**	**0.0014**	**45.41**	**0.0002**
Synthetic data 2						
Algorithm	SNR = 20 dB		SNR = 30 dB		SNR = 40 dB	
	SRE	RMSE	SRE	RMSE	SRE	RMSE
SUnSAL-TV	7.78	0.0296	13.08	0.0161	19.93	0.0073
ADSpLRU	7.49	0.0306	16.94	0.0103	26.46	0.0034
JSpBLRU	9.95	0.0230	18.74	0.0084	28.72	0.0027
BiJSpLRU	12.10	0.0180	20.13	0.0071	**29.64**	**0.0024**
MdLRR	**14.17**	**0.0142**	**21.37**	**0.0062**	29.25	0.0025

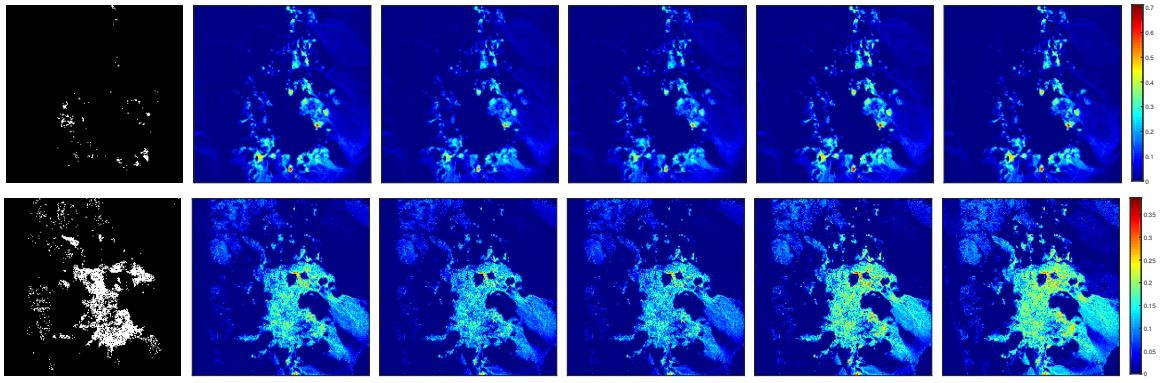

Fig. 7: Abundance maps estimated by different unmixing algorithms for (top row) Alunite and (bottom row) Chalcedony.

algorithms for Synthetic data 1 and 2 with SNR $= 30$ dB and SNR $= 20$ dB, respectively. As demonstrated in those figures, it is apparent that our approach not only preserves richer abundance information relative to the real abundance map but also removes more noise. The convergence process of the proposed algorithm regarding the SNR (dB) for the synthetic data 2 is shown in Fig. 6. Table I displays the SRE and RMSE values of different algorithms. The proposed MdLRR algorithm provides an improvement in SRE at least more than 1 dB except for one case (Synthetic 2 with SNR $= 40$ dB).

B. Real-data experiments

In our experiments, we choose the real data from the broadly used Airborne Visible/Infrared Imaging Spectrometer (AVIRIS) Cuprite dataset, that is, the Cuprite data with 350×350 pixels and 188 bands. We use the USGS spectral library to generate a spectral dictionary, and compare the abundance maps generated by various algorithms based on this dictionary. As discussed in [5–8], we set the parameters of SUnSAL-TV to $\lambda = \lambda_{\text{TV}} = 0.001$, the parameters of ADSpLRU, JSpBLRU, BiJSpLRU, and MdLRR are adjusted to $\lambda = \tau = 0.001$. Fig. 7 visualizes the reconstructed abundance maps. Due to the low noise of the real data, just subtle distinctions display in the abundance maps produced by different algorithms. Doubtlessly, our method still performs better in capturing the features of the real abundance map when compared to those efficient algorithms.

V. Conclusion

In this paper, we propose a multidimensional low-rank representation for the hyperspectral unmixing problem. Specifically, after reshaping the abundance matrix to an abundance tensor, we consider the low-rank property of abundance data through the three unfoldings by different modes. Moreover, we combine the multidimensional low-rank representation with the bilateral joint-sparse structure to exploit spectral and spatial information. We derive the MdLRR algorithm based on the ADMM framework. The experimental results demonstrate the proposed algorithm offers effective unmixing performance. In the future, we will keep investigating the use of sparse and low-rank priors in hyperspectral unmixing with plentiful information maintained in the hyperspectral data.

References

[1] N. Keshava and J. F. Mustard, "Spectral unmixing," *IEEE Signal Process. Mag.*, vol. 19, pp. 44–57, Jan. 2002.

[2] J. Bioucas-Dias *et al.*, "Hyperspectral unmixing overview: Geometrical, statistical, and sparse regression-based approaches," *IEEE J. Sel. Topics Appl. Earth Observ. Remote Sens.*, vol. 5, pp. 354–379, Apr. 2012.

[3] A. Plaza, P. Martinez, R. Perez, and J. Plaza, "A quantitative and comparative analysis of endmember extraction algorithms from hyperspectral data," *IEEE Trans. Geosci. Remote Sens.*, vol. 42, no. 3, pp. 650–663, 2004.

[4] D. C. Heinz *et al.*, "Fully constrained least squares linear spectral mixture analysis method for material quantification in hyperspectral imagery," *IEEE Trans. Geosci. Remote Sens.*, vol. 39, pp. 529–545, Mar. 2001.

[5] M.-D. Iordache, J. M. Bioucas-Dias, and A. Plaza, "Sparse unmixing of hyperspectral data," *IEEE Trans. Geosci. Remote Sens.*, vol. 49, pp. 2014–2039, June 2011.

[6] P. V. Giampouras, K. E. Themelis, A. A. Rontogiannis, and K. D. Koutroumbas, "Simultaneously sparse and low-rank abundance matrix estimation for hyperspectral image unmixing," *IEEE Trans. Geosci. Remote Sens.*, vol. 54, pp. 4775–4789, Aug. 2016.

[7] M.-D. Iordache, J. M. Bioucas-Dias, and A. Plaza, "Collaborative sparse regression for hyperspectral unmixing," *IEEE Trans. Geosci. Remote Sens.*, vol. 52, pp. 341–354, Jan. 2014.

[8] J. Huang, T.-Z. Huang, L.-J. Deng, and X.-L. Zhao, "Joint-sparse-blocks and low-rank representation for hyperspectral unmixing," *IEEE Trans. Geosci. Remote Sens.*, vol. 57, no. 4, pp. 2419–2438, 2019.

[9] J. Huang, W.-C. Di, J.-J. Wang, J. Lin, and T.-Z. Huang, "Bilateral joint-sparse regression for hyperspectral unmixing," *IEEE J. Sel. Topics Appl. Earth Observ. Remote Sens.*, vol. 14, pp. 10147–10161, 2021.

[10] M.-D. Iordache, J. M. Bioucas-Dias, and A. Plaza, "Total variation spatial regularization for sparse hyperspectral unmixing," *IEEE Trans. Geosci. Remote Sens.*, vol. 50, pp. 4484–4502, Nov. 2012.

[11] L. Sun, F. Wu, T. Zhan, W. Liu, J. Wang, and B. Jeon, "Weighted nonlocal low-rank tensor decomposition method for sparse unmixing of hyperspectral images," *IEEE J. Sel. Topics Appl. Earth Observ. Remote Sens.*, vol. 13, pp. 1174–1188, 2020.

[12] G. Kolda and B. W. Bader, "Tensor decompositions and applications," *SIAM Rev.*, vol. 51, no. 3, pp. 455–500, 2009.

[13] S. Boyd, N. Parikh, E. Chu, B. Peleato, and J. Eckstein, "Distributed optimization and statistical learning via the alternating direction method of multipliers," *Foundations and Trends in Machine Learning*, vol. 3, no. 1, pp. 1–122, 2011.